



Evidence of T -type structures of hard square boards in capillary confinementRoohollah Aliabadi ^{1,*}, Soudabe Nasirimoghadam ¹ and Henricus Herman Wensink²¹*Physics Department, Sirjan University of Technology, Sirjan 78137, Iran*²*Laboratoire de Physique des Solides - UMR 8502, CNRS, Université Paris-Saclay, 91405 Orsay, France*

(Received 4 November 2022; accepted 5 April 2023; published 17 May 2023)

We employ Onsager's second virial density functional theory combined with the Parsons-Lee theory within the restricted orientation (Zwanzig) approximation to examine the phase structure of hard square boards of dimensions ($L \times D \times D$) uniaxially confined in narrow slabs. Depending on the wall-to-wall separation (H), we predict a number of distinctly different capillary nematic phases, including a monolayer uniaxial or biaxial planar nematic, homeotropic with a variable number of layers, and a T -type structure. We determine that the favored phase is homeotropic, and we observe first-order transitions from the homeotropic structure with n layers to $n+1$ layers as well as from homeotropic surface anchoring to a monolayer planar or T -type structure involving both planar and homeotropic anchoring at the pore surface. By increasing the packing fraction, we further demonstrate a reentrant homeotropic-planar-homeotropic phase sequence in a particular range (i.e., $\frac{H}{D} = 1.1$ and $0.25 \leq \frac{L}{D} < 0.26$). We find that the T -type structure is more stable when the pore is wide enough with respect to the planar phase. The enhanced stability of the mixed-anchoring T -structure is unique for square boards and becomes manifest at pore width exceeding $L + D$. More specifically, the biaxial T -type structure emerges directly from the homeotropic state without intervention of a planar layer structure as observed for other convex particle shapes.

DOI: [10.1103/PhysRevE.107.054117](https://doi.org/10.1103/PhysRevE.107.054117)**I. INTRODUCTION**

Particle geometrical anisotropy shape is known to be a critical parameter in the formation of liquid crystalline phases such as smectic, nematic, and columnar phases [1]. Thanks to their significance in the construction of transistors and biosensors, and the development of novel materials with new physical characteristics, anisotropic molecules have been modeled with simple geometrical shapes such as disks, cylinders, spherocylinders, lenses, rings, and ellipsoids. Their phase behavior has been widely studied using simulation as well as theoretical approaches [2–4].

Hard disk-shape particles are an interesting case in point. With a rise in packing fraction, thin disks display nematic, isotropic, and columnar liquid crystalline phases, whereas thicker disklike particles may form a cubic rather than a nematic phase [2,5–7]. New phases such as hexatic and smectic B can also be stabilized through shape biaxiality, polydispersity, gravity, and surface charges [8–11].

Clearly, being able to control the alignment of oblate particles is crucial in applications that involve disklike liquid crystalline moieties, such as optical devices and photovoltaics [12]. In experiments, the number density and temperature of the particles are common parameters for particle alignment control [13]. These parameters can be regulated by setting the temperature and the strength of extrinsic interactions (wall-particle). According to Pineiro *et al.*, tuning a hard wall into an adsorbent wall helps switch discotic particles' surface

ordering from homeotropic (where the nematic director is perpendicular to the walls, or the disk diameters are parallel to the walls) to planar (where the nematic director is parallel to the walls, or the disk diameters are perpendicular to the walls) [14]. Whereas hard walls facilitate capillary nematization, adsorbing walls tend to postpone the formation of nematic structures [15]. Disk-shaped molecules can be modeled as impenetrable objects [14,16,17] or as a soft repulsive body [18] in terms of Gay-Berne-type oblate ellipsoids [19]. In most studies, density was the only control parameter, but the impact of density on the surface ordering was found to be marginal. In this paper, we show that increasing the overall particle density can have a serious impact on capillary structures formed by the disks.

Disk-shaped particles in strong planar confinement exhibit fascinating phases, including planar (P) and homeotropic (H) structures, as well as interesting characteristics such as homeotropic anchoring with complete wetting, or a capillary-induced isotropic-nematic transition that terminates at a pore width on the order of $\sim 4D$, where D denotes the disk diameter [14,17,20]. On the other hand, stiff ring polymers exhibit planar ordering as their preferred anchoring in the vicinity of a wall, which could be the result of the rings' penetrable nature [15,21]. Schoen and co-workers have examined the impacts of various extrinsic interactions on the stratification (layering structures) of confined particles with different molecular fluids using simulation [22,23]. They confirmed that stratification is not sensitive to the particle-wall interaction; for instance, hard spheres that were confined between hard walls [23] or soft Lennard-Jones particles that were constrained between molecularly structured and unstructured

*aliabadi313@gmail.com

walls [23,24] all developed layering structures. Furthermore, Khadiilkar and Escobedo observed layered structures of hard cubes in very narrow slitlike pores at intermediate densities [25]. Schoen *et al.* predicted that for structureless walls the formation of successive layers upon increasing particle crowding happens gradually without the occurrence of a phase transition [26,27]. Recent work by some of us demonstrated the existence of a first-order nematic layering transition for confined hard parallelepipeds and hard disks with a square cross-section between two structureless hard walls [28–30] where the structures of highly confined rods and disks are examined. Furthermore, nematic layering transitions were observed in narrow enough pores where the structure evolves from a nematic structure with n layers to a nematic structure with $n + 1$ layers.

In the current study, using the Parsons-Lee (PL) theory within the Zwanzig approximation or the restricted orientation model (ROM), we study the homeotropic layering transition from n to $n + 1$ layers, the transition from homeotropic structure with $n + 1$ layers to the planar structure with one layer, and the formation of a T -type structure (a combined structure with a planar and a homeotropic layer) of hard board-shaped particles with a square cross-section confined in very narrow pores. Based on previous studies, the ROM describes the fundamental physics of systems and qualitatively reproduces the findings of much more challenging models based on continuous particle orientations. The studies of Refs. [31,32] confirmed the qualitative validity of many Zwanzig model predictions of the phase behavior for numerous colloidal particles. In addition, Rickayzen [33] noted that the ROM does not seriously affect the results of confined hard rods. Still, the ROM may lead to quantitative deviations from continuous orientation models. Also, employing density functional methods based on the ROM may overestimate phase-transition densities, indicating the presence of an artificial aligned isotropic or nematic phase [34]. This problem can be overcome by adopting a theory to analyze the system in a freely rotating state. To prevent the creation of complex structures and the relaxation to the bulk properties in the pore center, we select the pore width such that the plates can establish homeotropic alignments with several layers, while only a single layer can form in the pore in the planar alignment. The exception is when we examine the formation of the T phase, in which case the pore can be wider to spontaneously form a planar and a homeotropic layer. The PL theory cannot consider solid phases; therefore, we did not examine the possible crystalline in-plane and out-of-plane phases. As a result, the confined fluid may freeze first and then transform into a new structure. This phenomenon is even more probable when the packing fraction of the particles is greater than 0.75, a case that is discussed in detail in the Conclusion.

II. THEORY

We study the orientational ordering of the hard square plates with a length of the short side L and a cross-section with edge length D constrained between two parallel hard structureless walls normal to the z -axis with wall-to-wall separation H (i.e., the walls are at $z = 0$ and $z = H$). All the interactions in the system are strictly hard; therefore,

the molecules are not allowed to penetrate each other, and the system walls are athermal and all structures are purely entropy-driven. To determine the examined structures of the confined hard disks at elevated particle packing fractions, we applied Parsons-Lee theory [35,36] for strongly confined system with pore distance $L < H \leq (L + D)$. Although PL theory is approximate, it accurately reproduces simulation results reported for bounded liquid crystalline particles in the quasi-one-dimensional (Q1D) limit [37,38]. We apply a three-state Zwanzig approximation [39], in which the main symmetry axes of the molecules are restricted to align along the three Cartesian directions (x , y , and z) equivalent to a ternary mixture of hard rods with no rotational degrees of freedom.

The external potential is a function of z alone, and we do not consider possible in-plane positional order. Then, the local density components (ρ_i , $i = x, y$, and z) depend only on the distance z from the walls. To determine the density components in inhomogeneous fluids, we define the PL grand-canonical free energy $\Omega[\rho]$ as follows:

$$\begin{aligned} \frac{\beta\Omega[\rho]}{A} = & \sum_{i=x,y,z} \left[\int dz \rho_i(z) (\beta V_{\text{ext}}^i(z) - \beta\mu) \right. \\ & \left. + \int dz \rho_i(z) (\ln \rho_i(z) - 1) \right] \\ & + \frac{1}{2} c \sum_{i,j=x,y,z} \int dz_1 \rho_i(z_1) \int dz_2 A_{\text{exc}}^{ij}(z_1 - z_2) \\ & \times \rho_j(z_2), \end{aligned} \quad (1)$$

where βV_{ext}^i denotes the external potential for a disk with orientation i , and μ represents the chemical potential. Moreover, $\beta = 1/(k_B T)$ and $c = (1 - 3\eta/4)/(1 - \eta)^2$ is the PL prefactor, whereas A_{exc}^{ij} denotes the excluded area in the $x - y$ plane between two disks with orientations i and j . The excluded areas between two disks for all possible combinations of orientations in Eq. (1) in the Zwanzig model can be found in Ref. [40].

The surface-disk interactions are different for particles aligning parallel (x and y orientations) and perpendicular (z orientation) to the walls,

$$\beta V_{\text{ext}}^x(z) = \beta V_{\text{ext}}^y(z) = \begin{cases} 0, & D/2 \leq z \leq H - D/2, \\ \infty & \text{otherwise} \end{cases} \quad (2)$$

and

$$\beta V_{\text{ext}}^z(z) = \begin{cases} 0, & L/2 \leq z \leq H - L/2, \\ \infty & \text{otherwise.} \end{cases} \quad (3)$$

The packing fraction (η) in the PL prefactor can be obtained from the density components through the following

equation:

$$\eta = \frac{v_0}{V} \sum_{i=x,y,z} \int d\vec{r} \rho_i(\vec{r}) = \frac{v_0}{H} \left(\int_{D/2}^{H-D/2} \rho_x(z) dz + \int_{D/2}^{H-D/2} \rho_y(z) dz + \int_{L/2}^{H-L/2} \rho_z(z) dz \right), \quad (4)$$

where $v_0 = LD^2$ is the volume of a disk, and $V = AH$ indicates the volume of the pore. Moreover, A is the area of the confining walls.

To determine the equilibrium local densities, the free energy of Eq. (1) must be minimized with respect to all the density components. Functional differentiation of the free energy leads to the following equation:

$$\begin{aligned} \ln \rho_k(z) - \beta\mu + \beta V_{\text{ext}}^k(z) + \frac{1}{2} \frac{dc}{d\eta} \frac{\delta\eta}{\delta\rho_k(z)} \sum_{i,j=x,y,z} \int dz_1 \rho_i(z_1) \int dz_2 A_{\text{exc}}^{ij}(z_1 - z_2) \rho_j(z_2) + \frac{(1-3\eta/4)}{(1-\eta)^2} \\ \times \sum_{i=x,y,z} \int dz_1 A_{\text{exc}}^{ik}(z - z_1) \rho_i(z_1) = 0, \end{aligned} \quad (5)$$

where $k = x, y, z$, $dc/d\eta = (5-3\eta)/4(1-\eta)^3$, and $\delta\eta/\delta\rho_k(z) = v_0/H$. The local density components can be rearranged into

$$\begin{aligned} \rho_k(z) = \exp \left[\beta\mu - \frac{v_0(5-3\eta)}{8H(1-\eta)^3} \sum_{i,j=x,y,z} \int dz_1 \rho_i(z_1) \int dz_2 A_{\text{exc}}^{ij}(z_1 - z_2) \rho_j(z_2) \right] \\ \times \exp \left[-\frac{(1-\frac{3\eta}{4})}{(1-\eta)^2} \sum_{i=x,y,z} \int dz_1 A_{\text{exc}}^{ik}(z - z_1) \rho_i(z_1) - \beta V_{\text{ext}}^k(z) \right], \quad k = x, y, z. \end{aligned} \quad (6)$$

Equation (6) has to be solved numerically using iterative methods at the given values of L/D , H/D , and $\beta\mu$. Since we prefer to work at a fixed packing fraction instead of chemical potential, the local density equations are defined in terms of η by substituting Eq. (6) into Eq. (4), extracting $\exp[\beta\mu]$, replacing it in Eq. (6), and finally inserting it into Eq. (4):

$$\rho_k(z) = \frac{H\eta \exp \left[-\beta V_{\text{ext}}^k(z) - \frac{(1-\frac{3\eta}{4})}{(1-\eta)^2} \sum_{i=x,y,z} \int dz_1 A_{\text{exc}}^{ik}(z - z_1) \rho_i(z_1) \right]}{v_0 \sum_{q=x,y,z} \int dz_1 \exp \left[-\beta V_{\text{ext}}^q(z_1) - \frac{(1-\frac{3\eta}{4})}{(1-\eta)^2} \sum_{i=x,y,z} \int dz_2 A_{\text{exc}}^{iq}(z_1 - z_2) \rho_i(z_2) \right]}, \quad k = x, y, z. \quad (7)$$

Equation (7) can be solved numerically for given values of L/D , η , and H/D by discretizing the z -interval on equidistant grid points ($\Delta z = \frac{H}{n}$, $z_i = i\Delta z$, $i = 0, \dots, n$) and using Picard's iteration methods based on a linear combination rule that mixes the results of successive iterations. We apply the criterion $\frac{1}{n+1} \sum_{i=0}^n \sum_{k=x,y,z} |\rho_k^{q+1}(z_i) - \rho_k^q(z_i)| < 10^{-10}$ to ensure convergence of the iteration after the q th iteration step. A discussion about the reliability of the convergence of successive iteration methods and discretization applied for the Euler-Lagrange integral equations can be found in Ref. [41].

A grid size of $\Delta z = 0.005$ is used whenever phase separation is expected to be strong. Smaller step sizes used ($= 0.001$ or 0.0001) in case the coexisting densities are very close. In the iterative numerical procedure, selecting a suitable initial value is important to guarantee reliable solutions for each phase. For example, $\rho_x = \rho_y = 0$ and $\rho_z > 0$ are chosen for the H structure. For the planar phase, $\rho_x > \rho_y > 0$ and $\rho_z = 0$ are selected. Although there is no difference between the x and y orientations, local trial densities are chosen so that they can result in $\rho_x \geq \rho_y$ to capture the biaxial structure in the system ($\rho_x \neq \rho_y$). To allow for T -type structures, we start from the planar configuration at one wall and the homeotropic configuration at another wall. To calculate the integrals, the trapezoidal quadrature method is used. It is possible to find more than one phase at a certain packing fraction; however,

the stable phase in the system is the one with the lowest free energy. For determining the coexistence region of a first-order phase transition, we should cross two different solutions of the free-energy equation in the plane $\beta\mu - \frac{\beta F}{A}$, then find the corresponding packing fractions. Furthermore, at a certain packing fraction, the stable phase is the one with the lowest free energy.

In the next section, we will show the obtained phase diagrams and density profiles for a number of different pore widths. All results are presented in dimensionless units, where D is the unit of distance, i.e., $\rho^* = \rho D^3$ and $z^* = z/D$.

III. RESULTS AND DISCUSSION

We examine the nematic structures of hard square disks confined between two structureless parallel hard walls in which the wall-to-wall separation is constant, while L/D is variable. The following cases will be studied specifically:

- (i) $H < D$: Here, we examine the structures of $\frac{H}{D} = 0.95$, where the planar (P) and T structures are not formed due to strong confinement; the prevalent ones are H structures with different numbers of layers.
- (ii) $D < H < D + L$ and $L > H/2$: We examine the phase structures of $\frac{H}{D} = 1.2$ and $\frac{L}{D} > 0.6$, where only a homeotropic or a planar layer is formed.

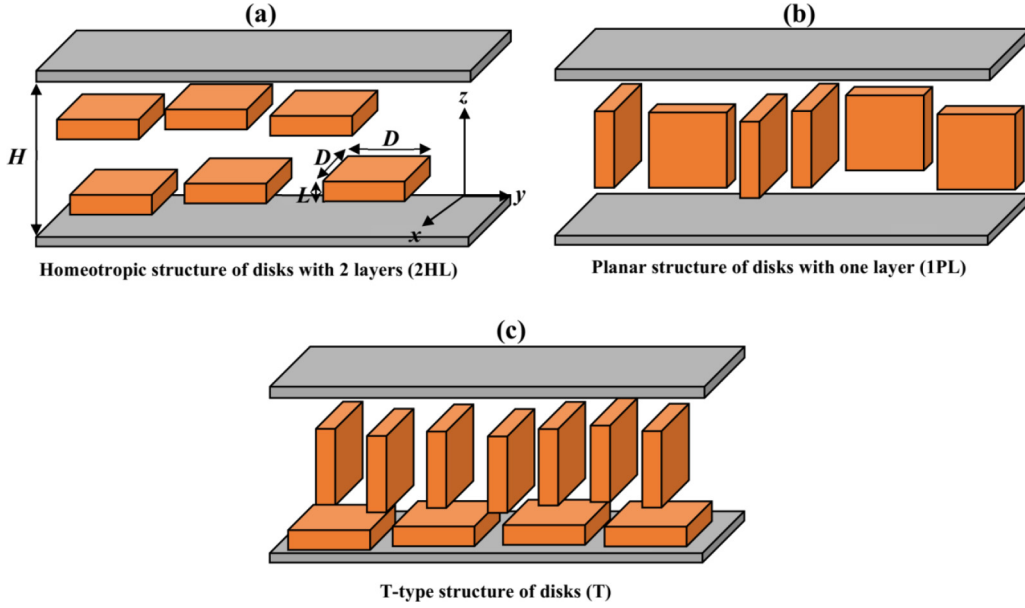


FIG. 1. Schematic representation of studied phase structures: (a) a homeotropic system with two layers denoted 2HL, (b) a single planar layer (1PL), and (c) the T -type structure.

- (iii) $D < H < D + L$ and $L < H/2$: We investigate the phase structures of $\frac{H}{D} = 1.1$ and $\frac{L}{D} < 0.55$, where both a planar layer and a homeotropic state with $n + 1$ layers (at maximum) are possibly stable. Thus, contrary to case (ii), in this case the competing structures are $(n)H - (n + 1)H$ and $(n + 1)H - 1P$.
- (iv) $H > D + L$: We study the phase structures of $\frac{H}{D} = 1.4$, where a planar layer, homeotropic with $(n + 1)$ layers, and T phase can form in the pore. In this case, all phases are competing for stability.

Figure 1 schematically depicts the structures considered in our study. All the structures are entropy-driven only to maximize the particle translational entropy and the available space. As such, the packing entropy term of the free energy Eq. (1) prefers to form phase structures with a lower excluded volume when the overall packing fraction exceeds a certain critical value.

We may compute maximum allowed packing fraction η for each examined structure to estimate its mechanical stability. Recalling the definition of the packing fraction ($\eta = \frac{Nv_0}{V}$), for example, if the phase consists of $n + 1$ layers in H order, the packing fraction can be factorized into two-dimensional (2D) and one-dimensional (1D) packing fractions as follows: $\eta = \eta_{2D}\eta_{1D}$, where $\eta_{2D} = \frac{ND^2}{(n+1)A}$ and $\eta_{1D} = \frac{(n+1)L}{H}$, and we will find $\eta_H = \frac{ND^2}{(n+1)A} \frac{(n+1)L}{H}$, where η_H is the packing fraction of H state and $n + 1$ denotes the maximum number of H layers that can be accommodated in the pore. To calculate the maximum packing fraction for this phase, the wall surface (i.e., A) should be completely covered with the particle side that is parallel to the walls. As squares arranged in a square lattice can perfectly cover a 2D surface (i.e., A), then $(\eta_{2D})_{\max} = 1$, consequently, the close packing fraction value is $(\eta_H)_{\max} = \frac{(n+1)L}{H}$. Similarly, one can obtain $\eta_P = \frac{NLD}{A} \frac{D}{H}$ and $\eta_T = \frac{ND^2}{A} \frac{L}{H} + \frac{NLD}{A} \frac{D}{H}$

for P and T phases, and their close packing fractions are $(\eta_P)_{\max} = \frac{D}{H}$ and $(\eta_T)_{\max} = \frac{L}{H} + \frac{D}{H}$, respectively. A comparison of these close packing values allows us to qualitatively discuss the stability of these phases. For instance, because $\frac{(n+1)L}{H} < \frac{D}{H}$, the stable phase is planar at high densities where only a homeotropic and a planar layer can form. However, when the pores are wide enough to accommodate the T -type phase, we find that this phase preempts the planar phase at high packing fraction. We demonstrate the consistency of the qualitative predictions by comparing against numerical results based on the free energy [Eq. (1)].

A. $H < D$

We now examine the phase structures that emerge when the wall separation is smaller than D yet larger than $2L$ (i.e., $2L < H < 1D$); in these cases, the disks can only accommodate H structures with a maximum of $n + 1$ layers and a minimum of two layers due to the strong particle-wall adsorption. The disks' preferred anchoring is H with strong adsorption at the walls because this type of ordering reduces the excluded area next to the walls. The adsorbed layers at the walls are uniaxial; as such, a tetratic structure and solid phases can form in these layers if their densities exceed the transition densities of two-dimensional (2D) hard squares [42–44]. For instance, for $0.316 < \frac{L}{D} < 0.475$ at the pore width of $\frac{H}{D} = 0.95$, the sole nematic structure that can exist is a homeotropic structure with two layers (2HL) that can undergo in-plane structures such as tetratic or solid phases by raising the packing fraction (which we do not discuss here). Results obtained from the phase equilibrium conditions and the transition densities of the coexisting phases are depicted in Fig. 2 for $\frac{H}{D} = 0.95$ and aspect ratios of $\frac{L}{D} < 0.316$, in which a pore $nHL - (n + 1)HL$ transition can occur.

As the aspect ratio drops, the maximum number of homeotropic layers that can form in the pore increases. To

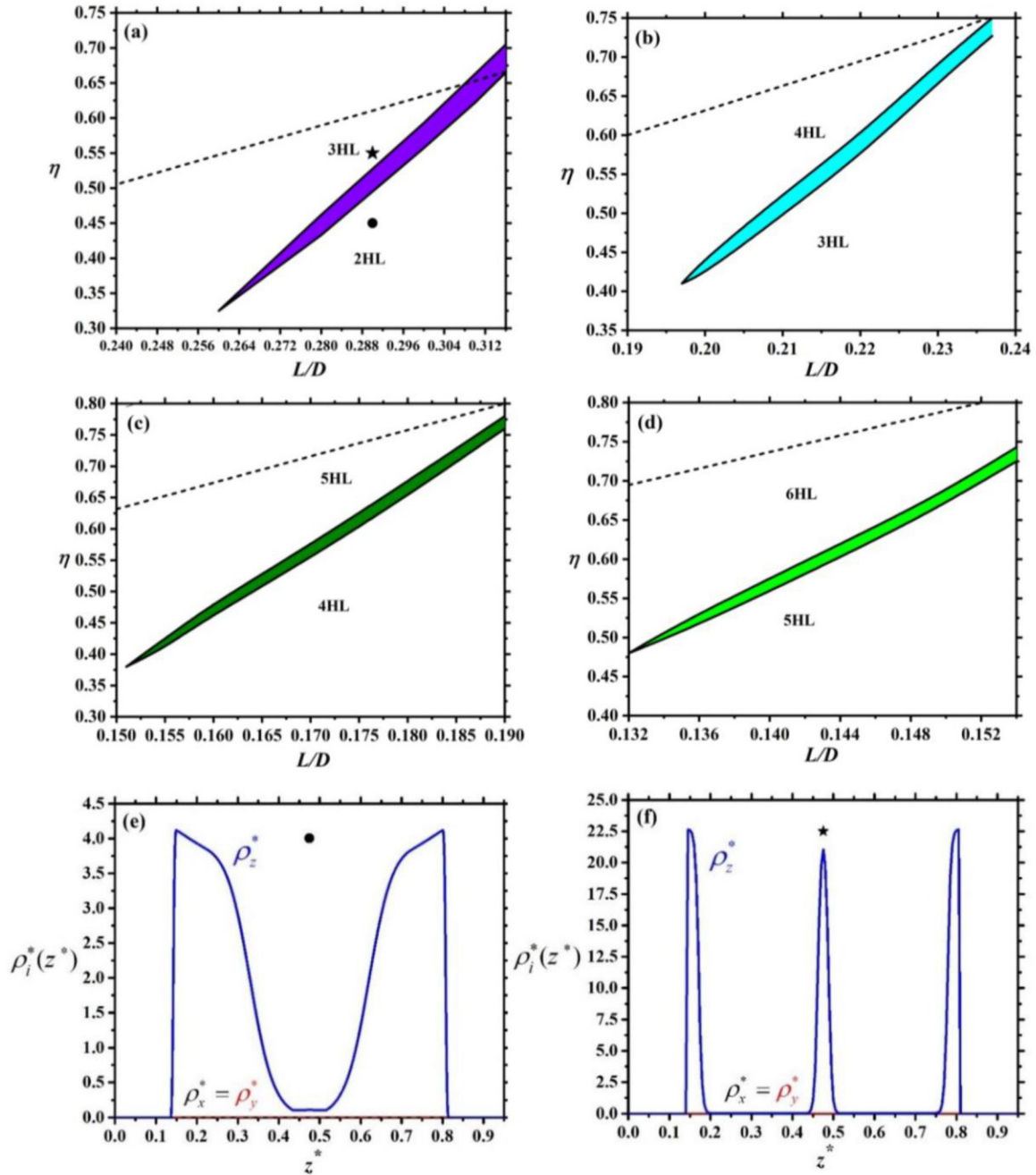


FIG. 2. Phase diagrams of $\frac{H}{D} = 0.95$ for homeotropic structures with different numbers of layers: (a) $\frac{L}{D} < 0.316$ featuring a 2HL-3HL transition; (b) $\frac{L}{D} < 0.237$ with 3HL-4HL; (c) $\frac{L}{D} < 0.19$ with 4HL-5HL; (d) $0.132 \leq \frac{L}{D} \leq 0.154$ with a first-order transition, i.e., 5HL-6HL; (e) density profiles related to filled circle symbol in panel (a), i.e., $(\frac{L}{D}, \eta) = (0.29, 0.45)$, where the phase is homeotropic with two thick adsorbed layers at the walls; and (f) density profiles related to the filled star symbol in panel (a), i.e., $(\frac{L}{D}, \eta) = (0.29, 0.55)$, where the phase is homeotropic with three sharp layers. The black dashed lines in (a), (b), (c), and (d) show the close packing fractions of 2HL, 3HL, 4HL, and 5HL phases, respectively.

form a maximum of three homeotropic layers in the pore, the aspect ratio must be less than ~ 0.316 ; thus, the first-order transition from the H structure with two layers to the H one with three layers (2HL-3HL) is displayed in Fig. 2(a), colored purple. Based on Fig. 2(a), there is a first-order transition between 2HL and 3HL for $0.26 < \frac{L}{D} < 0.316$ because the formation of a new H layer coincides with pushing the existing layers to the direction of the walls, and thus less space for old layers. This transition terminates at a criti-

cal $(\frac{L}{D})_c \approx 0.26$. For $\frac{L}{D} < (\frac{L}{D})_c$, the structure continuously varies from 2HL to 3HL because the particles can be accommodated into the pore more easily with three layers. The black dashed line in Fig. 2(a) displays the maximum packing fraction of the 2HL phase. Evidently, the 3HL state is stabilized before the packing fraction reaches this line; this means that 3HL is a highly stable phase. The maximum packing fraction of 3HL [i.e., $(\eta_H)_{\max} = \frac{3L}{0.95} > 0.75$] falls out of the given range. To steer clear of in-plane crystal-

lization, we depict some phase diagrams corresponding to packing fractions below ~ 0.75 . In general, any system at a packing fraction above 40–50 % has a tendency to display in-plane crystallization; however, in experimental studies there is a particle size dispersity that usually strongly suppresses the formation of crystal phases [45,46]. Figures 2(e) and 2(f), respectively, show the density profiles of the two packing fractions at $(\frac{L}{D}, \eta) = (0.29, 0.45)$ and $(0.29, 0.55)$, which can be identified by different symbols in Fig. 2(a). Based on Figs. 2(b), 2(c), and 2(d), there are similar nematic homeotropic first-order layering transitions for thinner disks, colored cyan, green, and yellow green, respectively, in which the maximum number of layers rises by decreasing L/D . In all these transitions, there is a critical aspect ratio where the first-order phase transition terminates. Some critical points take place in the range where one can expect to observe $n\text{HL}-(n+1)\text{HL}$ and $(n+1)\text{HL}-(n+2)\text{HL}$ spontaneously. There is a range of L/D i.e., $0.150 \leq \frac{L}{D} \leq 0.154$, where a sequence of homeotropic layering transition occurs where $4\text{HL}-5\text{HL}$ and $5\text{HL}-6\text{HL}$ first-order transitions take place by increasing the packing fraction. The dashed lines in Figs. 2(b), 2(c), and 2(d) denote the close packing fractions of 3HL , 4HL , and 5HL , in that order. A competition between $n\text{HL}$ and $(n+1)\text{HL}$ may arise when the opposite walls induce oscillatory layered structures interfering with each other. As for homeotropic with n layers ($n\text{HL}$), the translational entropy has an important contribution, while the packing entropy plays a minor role given that the layers are rather wide. On the other hand, for the $(n+1)\text{HL}$ structure, excluded volume correlations are very strong and the density profile within the layers is quite sharp.

B. $D < H < L + D$ and $L > H/2$

In this section, we examine disks with $\frac{L}{D} > 0.6$, where $1 < H/D < L/D + 1$, in which only one H or one P layer can form; hence, the local densities do not depend on z . Here, we can consider three structures: 1HL , 1PL (the disks in the planar state have $\rho_x = \rho_y$, i.e., the phase is uniaxial), and 1BPL (the disks with a planar orientation have $\rho_x > \rho_y$, i.e., the phase is biaxial). The mole fraction curves ($X_i = \frac{\int dz \rho_i(z)}{\sum_{j=x,y,z} \int dz \rho_j(z)}$, $i = x, y, \text{ and } z$) are plotted versus the packing fraction in Figs. 3(a), 3(b), and 3(c), respectively, for $\frac{L}{D} = 0.6, 0.7, \text{ and } 0.8$. At lower densities, the number of particles in the H state is greater than the number of particles in planar ordering since the available room along the z direction is larger in the H state and the particles are easily adsorbed by the wall in the H phase. By increasing $\frac{L}{D}$, the value of X_z declines, yet the values of $X_x = X_y$ increase. There is a special intermediate packing fraction where the number of the particles in the planar state overtakes to minimize the excluded area between the plates. This happens at higher η for larger $\frac{L}{D}$. Figures 3(a), 3(b), and 3(c) demonstrate that the biaxiality of the planar phases ($X_x \neq X_y$) occurs at higher packing fractions by raising the aspect ratio of the particles. The stability regions of 1HL , 1PL , and 1BPL can be observed in Fig. 3(d) in the $\eta-L/D$ plane for $\frac{H}{D} = 1.2$. The black dashed solid line denotes a border where the fraction of particles in the H structure decreases compared to the particles in the P state

(i.e., $X_z < 0.5$) by increasing the packing fraction since the particles have more room in the P state. As an example, assume that we have shown point $X_z = 0.5$ by vertical and horizontal arrows in Fig. 3(a). Since mole fractions and thermodynamic quantities are continuously changing with packing fraction, this border does not show a real phase transition. 1HL destabilizes with respect to 1PL by raising the thickness of the rods since the contribution of the excluded volume entropy is increasing and the particles have more free volume (lower excluded area) in the 1PL order and, especially for $\frac{L}{D} \geq 0.8$, the stable phase is 1PL even at very low packing fractions. The solid red line indicates the second-order uniaxial planar-biaxial planar phase transition that happens at higher densities when $\frac{L}{D} \rightarrow 1$ since the shape anisotropy of the disks is decreasing.

The $1\text{HL}-1\text{PL}$ takes place in the normal fluid density regime, while the $1\text{PL}-1\text{BPL}$ transition occurs at $\eta > 0.75$, in which it is probably preempted by solidification. The black dashed line shows the close packing fraction of 1HL ; evidently, $\eta_{1\text{HL}-1\text{PL}}$ does not exceed this line. The black dotted line indicates the maximum packing fraction of 1PL . The $1\text{PL}-1\text{BPL}$ exceeds this line for $L/D \gtrsim 0.7$, which means that this structure is highly unstable for them. The density profiles of $\frac{L}{D} = 0.65$ are depicted in Figs. 3(e) and 3(f) at two packing fractions, i.e., $\eta = 0.1$, where the favored structure is 1HL and $\eta = 0.7$ in which the phase is 1PL . These points are denoted by different symbols in Fig. 3(d).

C. $D < H < D + L$ and $L < H/2$

To study more complex structures, we investigate the case $\frac{H}{D} = 1.1$ with $\frac{L}{D} < 0.55$, where $n+1$ homeotropic layers and one planar layer can form in the pore. One can expect $n - (n+1)$ homeotropic layering transitions, and $(n+1)\text{HL}-1\text{PL}$ and $1\text{PL}-1\text{BPL}$ transitions. In Fig. 4(a), the phase structure of $0.32 \leq \frac{L}{D} < 0.55$ is determined using the phase equilibrium conditions. For $0.37 \leq \frac{L}{D} \leq 0.55$, only 2HL and 1PL can form in the pore; therefore, we examine the phase transition between these two structures.

According to Fig. 4(a), there is an island where a first-order phase transition takes place from 2HL to 1PL (green region) for $0.314 \leq \frac{L}{D} \leq 0.44$. There are two critical points at $\frac{L}{D} \approx 0.44$ and $\frac{L}{D} \approx 0.314$ for this transition.

The blue solid line demonstrates the uniaxial-biaxial transition of the planar structure that occurs at higher densities at increasing aspect ratio (or a reduction in shape anisotropy) since in-plane ordering reduces the amount of volume exclusion. It is, however, more difficult to rationalize 2HL phase stabilization with respect to 1PL for thicker particles since the translational entropy is now larger in the planar order. The $2\text{HL}-1\text{PL}$ transition takes place below the blue line and the close packing densities of 2HL (black dashed line), exhibiting the high stability of the 1PL structure. The green horizontal dashed-dotted line shows the close packing densities of 1PL (or 1BPL). For more anisotropic hard plates [Fig. 4(b)], $0.22 \leq \frac{L}{D} < 0.32$, there are two phase regions, i.e., $0.22 \leq \frac{L}{D} \leq 0.25$ and $0.25 < \frac{L}{D} < 0.32$. In $0.22 \leq \frac{L}{D} \leq 0.25$ the $3\text{HL}-4\text{HL}$ (cyan region) and $4\text{HL}-1\text{BPL}$ (pink region) first-order phase transitions take place by increasing the packing fraction, both of which terminate at a critical

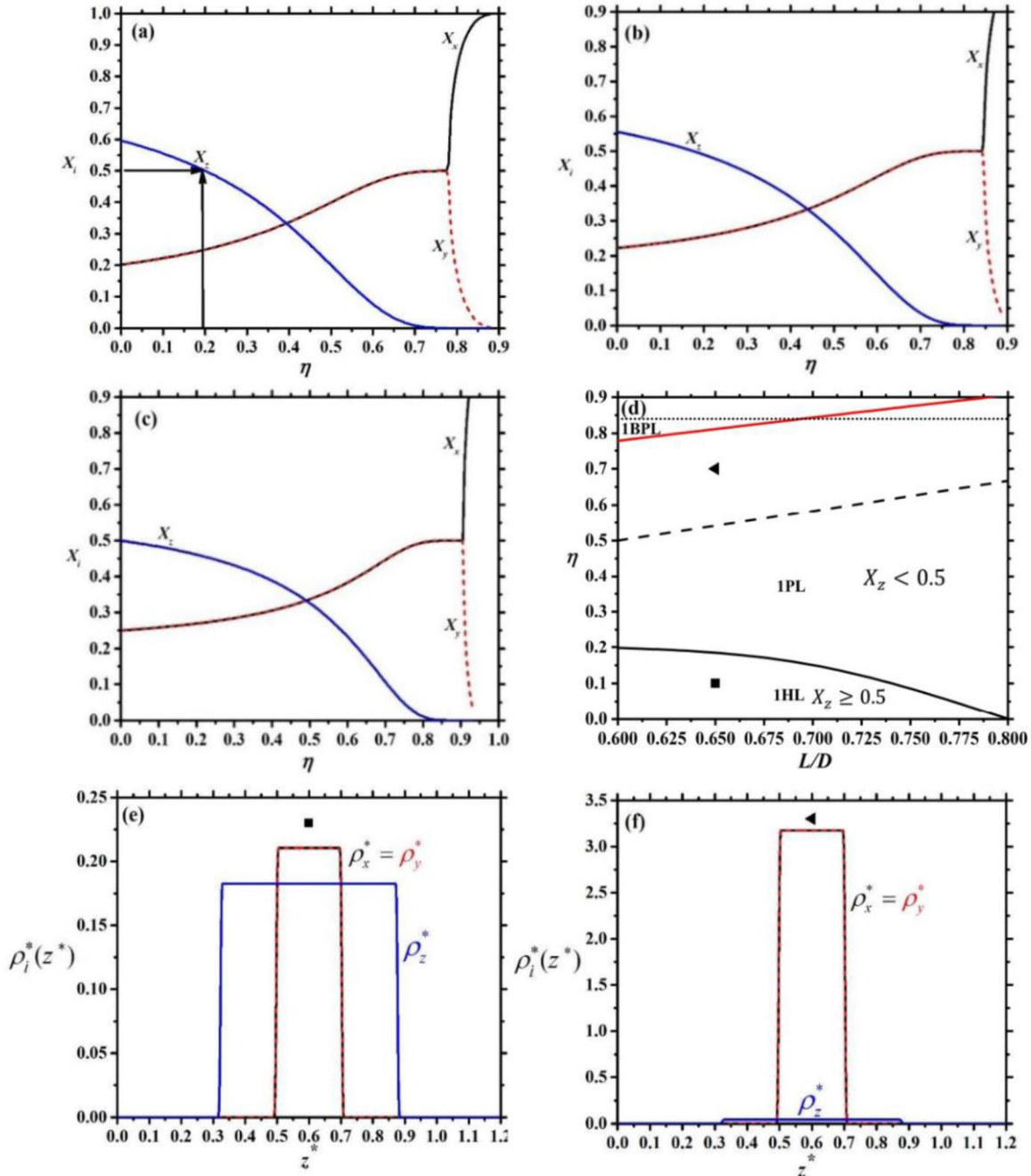


FIG. 3. Phase structures of $\frac{h}{D} = 1.2$ and $0.6 \leq \frac{l}{D} < 1$, where only one H or one P fluid layer is allowed to form (a) the mole fraction components of $\frac{l}{D} = 0.6$; (b) the mole fraction components of $\frac{l}{D} = 0.7$; (c) the mole fraction components of $\frac{l}{D} = 0.8$; (d) borders of the observed phases in the $\eta-L/D$ plane (the following phases are observed: 1HL, 1PL, and 1BPL); (e) the density profiles of $\frac{l}{D} = 0.65$ at $\eta = 0.1$, where its related point has been shown by a filled square in panel (d); and (f) the density profiles of $\frac{l}{D} = 0.65$ at $\eta = 0.7$, where its related point has been shown by a filled triangle in panel (d).

aspect ratio $\frac{l}{D} \approx 0.22$. The phase sequence is different for $0.25 < \frac{l}{D} < 0.32$, i.e., the first-order phase transition 3HL-1BPL (red region) occurs first, and then 1BPL-4HL (yellow green region) by increasing the packing fraction. Based on Fig. 4(b), the transition from n HL to the planar structure takes place at higher densities for thicker hard plates. According to the close packing argument, if $0.275 \leq \frac{l}{D} < 0.32$, the plates should be in a planar order at very high densities. Note that only 3HL and 1BPL can form in the pore for these

particles. This transition develops even for smaller aspect ratios, i.e., $0.25 \leq \frac{l}{D} \leq 0.275$, where 4HL can also form in the pore. There is a critical $(L/D)_c \approx 0.31$ in which first-order 3HL-1BPL terminates. This transition happens below the close packing densities of 3HL (black dashed line). The high-density stable phase is 4HL for $0.25 \leq \frac{l}{D} < 0.275$ because $\eta_{\max}(4HL) > \eta_{\max}(1BPL)$. These close packing fractions are denoted by a dotted black line and horizontal dashed-dotted line, respectively. Thus, an additional first-order transition

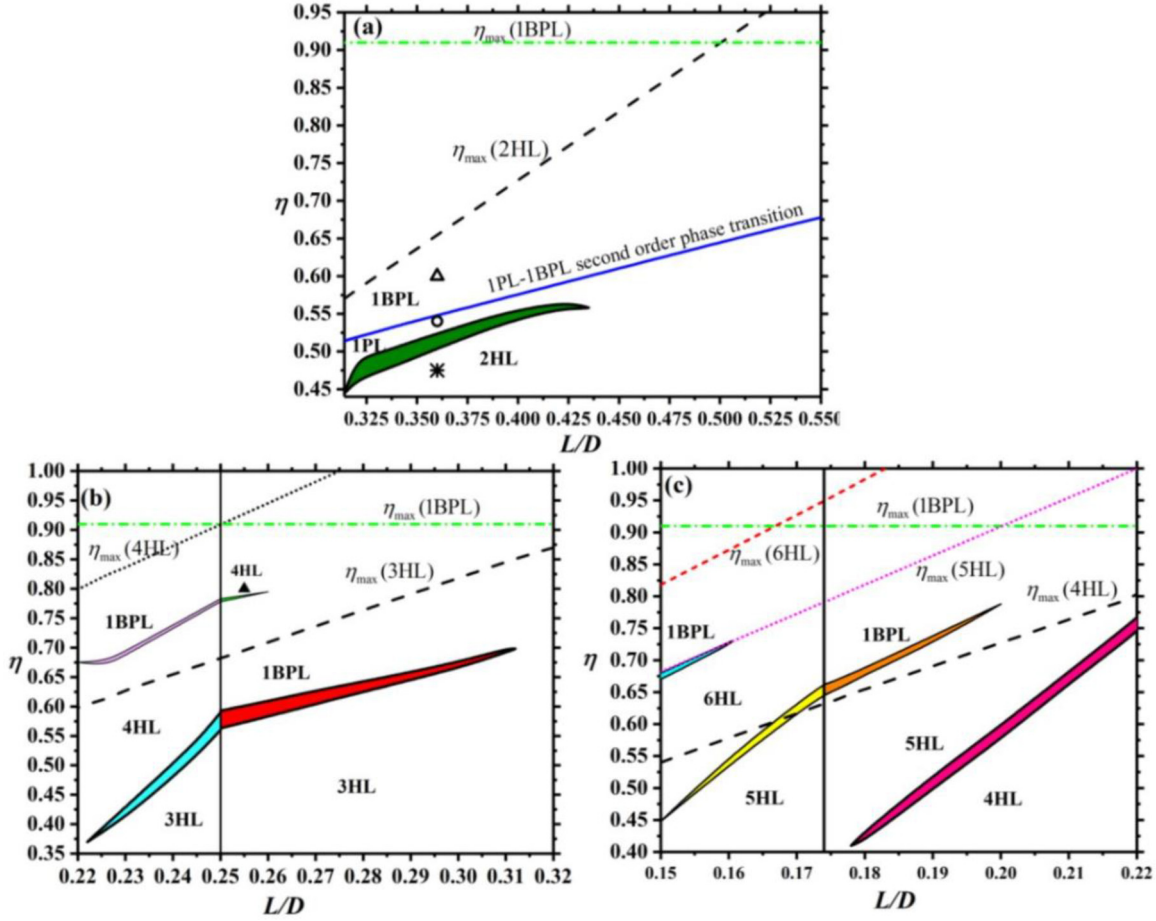


FIG. 4. Phase diagram of confined hard plates with $\frac{h}{D} = 1.1$: (a) $0.314 \leq L/D < 0.55$, where 2HL, 1PL, and 1BPL structures are formed; (b) $0.22 \leq L/D < 0.32$, with 3HL, 4HL, and 1BPL; (c) $0.15 \leq L/D < 0.22$, with 4HL, 5HL, 6HL, and 1BPL.

between 1BPL and 4HL (yellow green region) occurs at high densities. It means that in the $0.25 \leq \frac{L}{D} < 0.275$ range, the nematic director changes its direction twice by increasing the packing fraction, and a reentrant phenomenon occurs. Note that 1BPL-4HL takes place at very high densities where the system initially freezes and then changes from 1BPL to 4HL. This first-order phase transition occurs at a higher packing fraction by increasing $\frac{L}{D}$ since it is more difficult for thicker hard plates in the pore to accommodate four homeotropic layers and it terminates at a critical aspect ratio $L/D \approx 0.26$. The scenario is completely different for thinner disks, i.e., $0.22 < \frac{L}{D} < 0.25$, where $\eta_{\max}(4HL) < \eta_{\max}(1BPL)$. As mentioned here, the phase sequence is 3HL-4HL-1BPL by increasing the packing fraction. We depicted $\frac{L}{D} = 0.25$ in Fig. 4(b) by a vertical black solid line.

In Fig. 4(c), the phase structures of $0.15 \leq \frac{L}{D} \leq 0.22$ are plotted. Similar to Fig. 4(b), there are two phase regions here, i.e., $0.15 \leq \frac{L}{D} \leq 0.174$ and $0.174 \leq \frac{L}{D} \leq 0.22$. For thicker plates where $0.174 \leq \frac{L}{D} \leq 0.22$ there is a first-order layering transition from 4HL to 5HL (pink region) that takes place at lower densities by reducing $\frac{L}{D}$ and it stops at $\frac{L}{D} \approx 0.177$. In this range, 5HL is more stable at intermediate densities with respect to 1BPL as the close packing argument confirms this stability for $\frac{L}{D} < 0.199$ because $\eta_{\max}(5HL) < \eta_{\max}(1BPL)$. The pink dotted line stands for $\eta_{\max}(5HL)$ and the horizontal

yellow green dashed-dotted line indicates $\eta_{\max}(1BPL)$. Consequently, there is another first-order transition from 5HL to 1BPL (orange region) at higher densities. This transition happens at higher packing fractions by increasing $\frac{L}{D}$ and it ceases at $\frac{L}{D} \approx 0.199$. Similar phase transitions can be observed for $0.15 \leq \frac{L}{D} \leq 0.174$ where 5HL-6HL (yellow region) and 6HL-1BPL (cyan region) occur. According to the close packing argument, 6HL is also more stable than 1BPL for $0.15 \leq \frac{L}{D} < 0.167$, and this confirms the phase diagrams. Figure 5 displays the density profiles of the phases in Figs. 4(a) and 4(b) at four packing fractions denoted by different symbols. Figure 5(a) shows the density profiles of $\frac{h}{D} = 1.1$ and $\frac{L}{D} = 0.36$ at $\eta = 0.475$, where the structure is homeotropic with two layers with strong adsorption at the walls. By increasing the packing fraction, the number of particles in H state starts to drop; the number of particles with a P alignment increases; and the phase changes from 2HL to 1PL as evident from Figs. 4(a) and 5(b) at $(\frac{L}{D}, \eta) = (0.36, 0.54)$. With a further increase in the density, a second-order phase transition takes place and 1PL changes to 1BPL. Therefore, the phase is 1BPL at $(\frac{L}{D}, \eta) = (0.36, 0.60)$, where $\rho_x \neq \rho_y$ as evident from Figs. 4(a) and 5(c). Figure 5(d) exhibits the high-packing fraction phase in 4HL at $\frac{h}{D} = 1.1$, $\frac{L}{D} = 0.255$, and $\eta = 0.80$ whose symbol (a filled triangle) can be observed in Fig. 4(b).

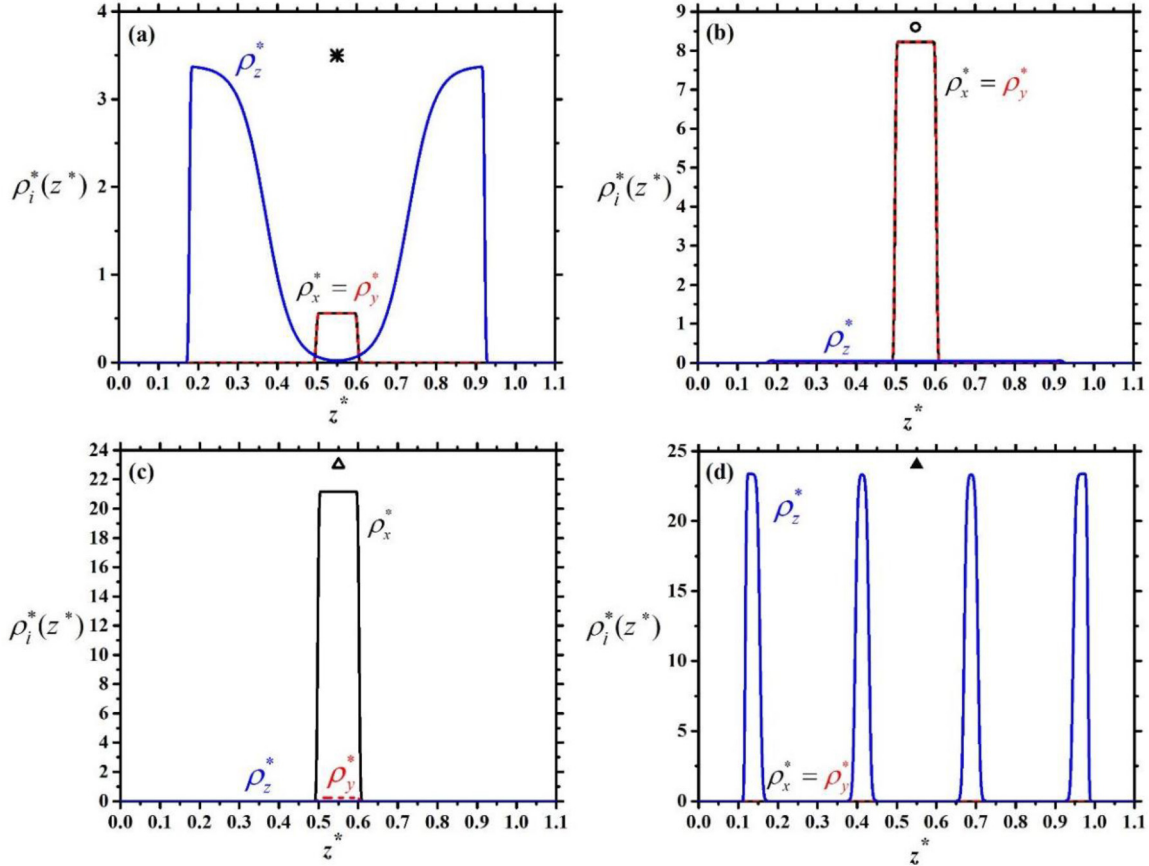


FIG. 5. Density profiles related to the symbols in Figs. 4(a) and 4(b). (a) $\frac{L}{D} = 0.36$ and $\eta = 0.475$, where the structure is 2HL; (b) $\frac{L}{D} = 0.36$ and $\eta = 0.54$, where the structure is 1PL; (c) $\frac{L}{D} = 0.36$ and $\eta = 0.6$, where the structure is 1BPL; (d) $\frac{L}{D} = 0.255$ and $\eta = 0.8$, where the structure is 4HL.

D. $H > D + L$

We have also examined wider pores where $(n + 1)HL$, planar structure, and *T*-type phase can form. The phase structures of $\frac{H}{D} = 1.4$ and $0.22 < \frac{L}{D} < 0.35$ are investigated in Fig. 6(a) where there are two phase regions, i.e., $0.22 < \frac{L}{D} \leq 0.27$ and $0.27 < \frac{L}{D} < 0.35$. For thicker particles ($0.27 < \frac{L}{D} < 0.35$) since the stable phases at intermediate packing fractions are 3HL and 4HL, a first-order layering transition (blue region) occurs by raising the packing fraction.

The wider part of this transition is in larger $\frac{L}{D}$ since it is more difficult to accommodate four layers of thicker hard plates in the pore. This transition ceases at a critical aspect ratio $\frac{L}{D} \approx 0.295$ where the phase change continuously occurs for smaller aspect ratios from 3HL to 4HL. For greater clarity, we have plotted the density profile of $\frac{L}{D} = 0.3$ [the plus symbol in Fig. 6(a) and the curves in Fig. 6(b)] in the range where there is a first-order phase transition between 3HL and 4HL. We have also shown the density profiles of $\frac{L}{D} = 0.29$ [the asterisk in Fig. 6(a) and its density profiles in panel (c)] where the phase continuously changes at the same packing fraction. To form the fourth layer from 3HL, the layer in the middle of the pore must be divided into two layers. For $\frac{L}{D} < (\frac{L}{D})_c = 0.295$, the layer is wide and can easily divide, and thus there is no phase transition here. Still, for $0.295 \leq \frac{L}{D} < 0.35$ this layer is not wide but relatively sharp; therefore, its division is

accompanied by pushing the existing layers to the walls and a first-order transition occurs.

In Fig. 6(a), the black dashed line, green dashed-dotted horizontal line, red short-dashed line, pink solid line, and blue dotted line, respectively, show $\eta_{\max}(3HL)$, $\eta_{\max}(1BPL)$, $\eta_{\max}(4HL)$, $\eta_{\max}(5HL)$, and $\eta_{\max}(T)$. The 1BPL and *T*-type structures compete at high densities; however, according to the close packing argument, since $\eta_{\max}(T) > \eta_{\max}(1BPL)$, the *T*-type structure is more stable with respect to 1BPL at high densities because the particles can be more packed by selecting the *T* structure rather than planar and homeotropic structures. The free-energy value of 1BPL is also higher than that of the *T* phase at high densities. Consequently, the more stable phase at high densities is *T* with respect to 1BPL, and the *n*HL structure directly changes into a *T*-type one. The *T* structure can be uniaxial or biaxial, yet the favored structure at high densities is a biaxial *T* phase (BT) because at such high densities, biaxiality provides a greater space for the particles near the wall. The density profiles of $\frac{L}{D} = 0.3$ at $\eta = 0.55$ and 0.725 are plotted in Figs. 6(d) and 6(e), where the phase is 4HL and BT, respectively. Evidently, the homeotropic particles are depleted from the middle of the pore at $\eta = 0.725$ [Fig. 6(e)] by increasing the packing fraction; both planar and homeotropic particles are adsorbed at the walls; and the segregation of the homeotropic and planar particles takes place at the opposite walls. In the $0.27 \leq \frac{L}{D} < 0.31$ range, the

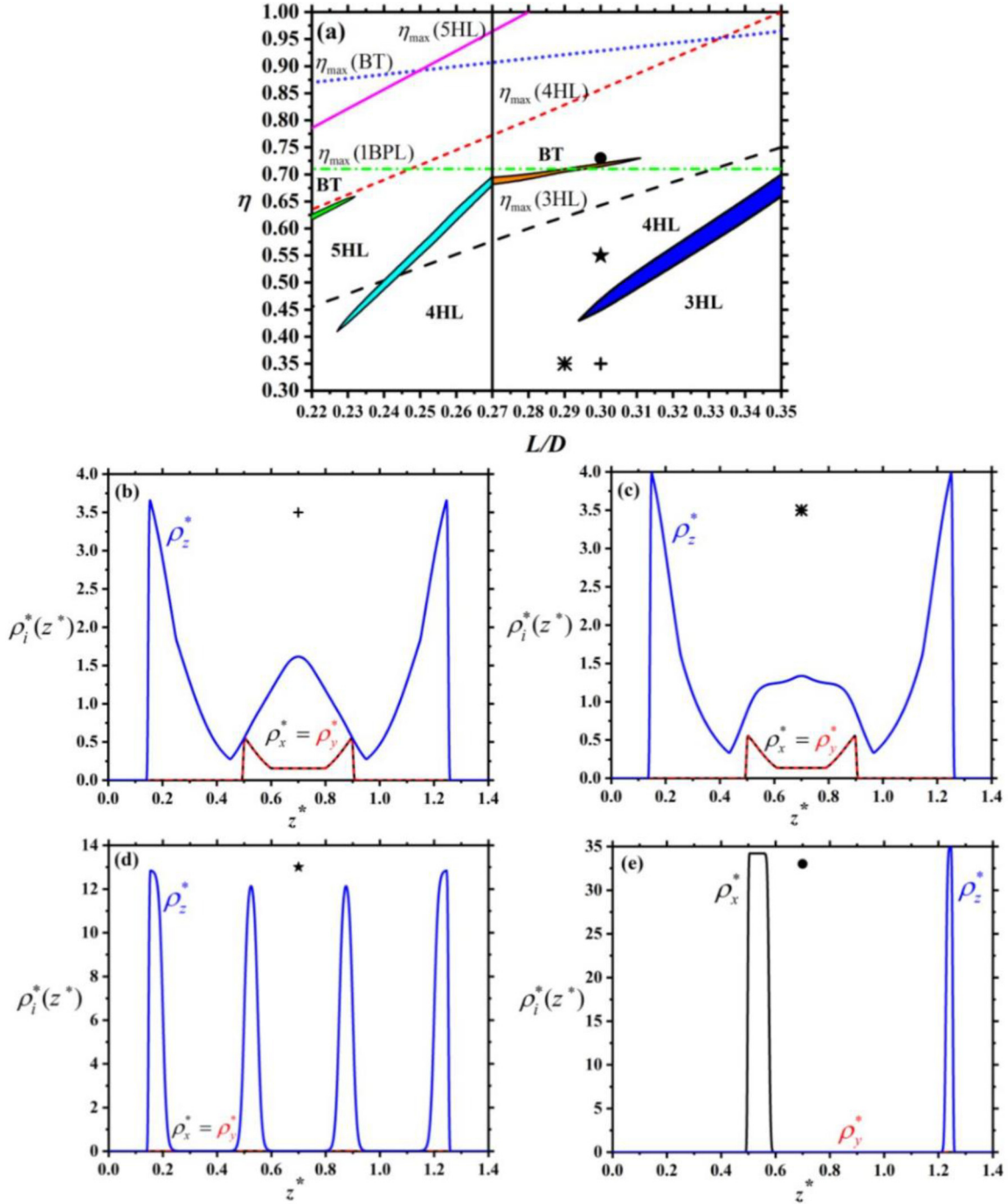


FIG. 6. (a) Phase diagram of $\frac{h}{D} = 1.4$ when $0.22 < \frac{L}{D} < 0.35$. Density profiles related to the symbols in panel (a) at (b) $(\frac{L}{D}, \eta) = (0.3, 0.35)$, where the phase is 3HL with a relatively sharp layer in the middle of the pore; (c) $(\frac{L}{D}, \eta) = (0.29, 0.35)$, where the phase is 3HL with a wide layer in the middle of the pore; (d) $(\frac{L}{D}, \eta) = (0.3, 0.55)$, where the phase is 4HL with very sharp layers; and (e) $(\frac{L}{D}, \eta) = (0.3, 0.725)$, where the phase is BT with a biaxial planar layer at a wall and a homeotropic one at the other wall.

structure changes from 4HL to T by a first-order transition [orange region in Fig. 6(a)] that becomes weaker with increasing L/D and takes place at higher packing fractions since it is more difficult to accommodate thicker disks in the T phase in the pore. This transition also stops at critical $(\frac{L}{D})_c \approx 0.31$. Similar phase transitions occur in $0.22 \leq \frac{L}{D} < 0.27$, where 5HL can form in the pore [Fig. 6(a)] where the first-order phase transitions 4HL-5HL (cyan region) and 5HL-BT (yel-

low green region) occur and they terminate at $\frac{L}{D} \approx 0.227$ and $\frac{L}{D} \approx 0.23$, respectively.

IV. CONCLUSION

The effects of the thickness of square disks and the pore width on their structural phases when they are constrained between two parallel hard walls were studied by using the PL

theory in a restricted orientation approximation. We focused on the strong confinement regime characterized by strongly inhomogeneous structures next to the walls, where the structures did not relax to their bulk structure even in the center of the system, and thus strong interference between the opposing walls was in charge of the observed phases. A theoretical examination of particles in very narrow pores can provide evidence for structures permissible for the quasi-2D regimes where the ordering resulting from the capillary characteristics becomes prominent [47].

We observed a uniaxial nematic order (homeotropic) with strong adsorption at the walls and different permissible numbers of layers, which was the preferred anchoring symmetry at low and intermediate densities. The strong surface adsorption decreases the excluded volume cost between the particles with this kind of ordering as it maximizes the space between the walls for the plates. As a result, homeotropic fluids that have n and $n + 1$ layers can undergo continuous first-order layering transitions. In several cases, the formation of a new homeotropic layer for thick-enough hard plates coincides with a first-order layering phase transition and high translational entropy costs. Capillary nematization does not influence the observed layering transitions since the capillary nematization critical point is observed at pore widths ($\sim 4D$) greater than the strongly confined cases here. The findings of the current study indicate that there are always two homeotropic layers at the walls when the pore is wide enough; nevertheless, there is a competition between a planar layer in the middle of the pore and a homeotropic layer. As such, the H phase changes to a P one for the cases that are not wide enough to form a *T*-type structure as the packing fraction rises. Planar ordering reduces the excluded volume at high packing fractions, thereby explaining the transition. The system triggers a transition from a uniaxial planar to a biaxial planar structure at a special packing fraction, resulting from pure repulsive extrinsic interactions, which is in line with Onsager's original findings [1]. This is generated by an exchange between excluded volume entropy and orientation entropy. Contrary to a previous study [29], we demonstrate that the biaxial nematic ordering (BT or BP) can be observed even in fluids of very anisotropic hard plates above $\eta > 0.5$ when $\frac{H}{D} > 1$. Note that the uniaxial planar structure (1PL) is observed only in the case of $\frac{H}{D} = 1.1$ and $0.314 \leq L/D < 0.55$ in which the transition from homeotropic to planar occurs at $\eta < 0.55$, where the second-order uniaxial-biaxial phase transition takes place at higher packing fractions by reducing the shape anisotropy due to the decreased packing entropy gain with in-plane ordering. In addition, biaxial order was reported for confined prolate and oblate particles [48]. For the other cases studied herein, the $(n + 1)$ HL phase replaces 1PL and the transition directly occurs from homeotropic to 1BPL as it takes place at $\eta > 0.55$. On the other hand, a planar to homeotropic transition is also reported in certain thermotropic systems [49]. We provide evidence for the formation of a biaxial *T* structure emerging from the homeotropic with $n + 1$ layers of confined hard square disks for $H > L + D$, where it overcomes the planar structure, and thus the phase sequence H-P-T is not observed in wide-enough pores. Martinez-Raton [50] investigated the bulk behavior of square disks but predicted no nematic structures when $0.25 < \frac{L}{D} < 1$. The formation of

the *T* structure is thus a capillary effect. Still, there is no preference for the particles to align parallel to a specific wall and perpendicular to the other as the two walls are identical; thus, in an experiment, one can expect to find domains of *T* and inverted *T* phases separated by domain walls. We also provide evidence for a concentration-driven reentrant H-P-H phase sequence when $\frac{H}{D} = 1.1$ and $0.25 \leq \frac{L}{D} < 0.26$.

We did not analyze potential in-plane and out-of-plane crystal phases as the PL theory cannot treat solid phases. Very narrow and sharp peaks through narrow pores can indicate capillary freezing, i.e., strong layering in confined fluids may initially freeze and then transform into new structures. At extreme confinement, when the pore distance is on the scale of the molecular size, solidlike phases could indeed develop. However, in experiments, size dispersity of the particles, which is naturally present in most colloidal system, usually impedes the formation of fully developed crystal phases [45,46].

In the future, the proposed model could be theoretically analyzed via fundamental measure theory (FMT) in the context of freely rotating nonspherical hard particles [51–53] and hard prolate and oblate parallelepipeds using the Zwanzig approximation [50]. This can be a major step forward since FMT has been demonstrated to be accurate for infinitely thin plates [54]. Structures with planar uniaxial or biaxial nematic layers and the presence of layering transitions reported in this study have also been found in theoretical, simulation, and experimental studies on confined liquid-crystal particles; as such, our predictions may qualitatively resemble those of freely oriented particles [26,55–57]. A surface forces apparatus was initially employed to observe the layered structure, and the layering structures were theoretically identified using the density dependence on position z between the walls. This phenomenon is a general effect of confinement that depends on the nature of intrinsic and extrinsic potentials. A detailed examination of Lennard-Jones molecules by Schoen and co-workers suggests that the structure and stiffness of walls considerably affect the layered structure [26,57]. Since the restricted-orientation model may stabilize the *T*-configuration of particles, caution should be taken when removing the restrictions in orientations on the stability of the confined *T* phase. Nevertheless, we believe that our results are qualitatively correct since cholesteric liquid crystal confined between two parallel walls has been reported to have *T*-type structure [58]; it has also been theoretically reported for parallelepipeds and cylinders [40,59], even at lower packing fractions with respect to hard square disks. There is no doubt that a special smectic phase (i.e., discotic smectic) [50,60] can be stabilized at bulk for certain aspect ratios when using the Zwanzig approximation; nevertheless, several simulations of hard particles in freely rotating modes report that this peculiar smectic is never stable. Hence, the stability of discotic smectic reported in Refs. [50,60] can be an artifact of the restricted orientations. A definite answer can be obtained by simulating freely rotating hard square disks in an extremely confined fluid.

The importance of attractive interactions in the stability of structures could also be included. For example, the transition of laponite platelike particles from vapor to liquid can be accurately modeled by adding special square-well pair potentials to the hard-body interactions [61,62]. In

concentrated systems, however, ordering effects are principally due to hard-core interactions [1,2] and we believe our model to be generally applicable to strongly confined molecules or colloidal particles with an (effective) board shape. In particular, given the prevalence of reconfigurable biaxial and T -shaped configurations emerging from the model,

we believe that our findings can be useful for designing bistable devices or fabricating pressure sensors based on particles dominated by hard-core exclusion [63]. Note that all the different phases reported in this paper are a consequence of $H \sim L$ and D . For much thicker films, i.e., $H \gg L$ and D , alignment will be homeotropic; see, e.g., Ref. [17].

-
- [1] L. Onsager, The effects of shape on the interaction of colloidal particles, *Ann. (N.Y.) Acad. Sci.* **51**, 627 (1949).
- [2] L. Mederos, E. Velasco, and Y. Martínez-Ratón, Hard-body models of bulk liquid crystals, *J. Phys.: Condens. Matter* **26**, 463101 (2014).
- [3] H. H. Wensink and C. Avendaño, Empty smectic liquid crystals of hard nanorings: Insights from a second-virial theory, *Phys. Rev. E* **94**, 062704 (2016).
- [4] G. Cinacchi and S. Torquato, Hard convex lens-shaped particles: Densest-known packings and phase behavior, *J. Chem. Phys.* **143**, 224506 (2015).
- [5] J. A. C. Veerman and D. Frenkel, Phase behavior of disklike hard-core mesogens, *Phys. Rev. A* **45**, 5632 (1992).
- [6] R. Blaak, D. Frenkel, and B. M. Mulder, Do cylinders exhibit a cubatic phase? *J. Chem. Phys.* **110**, 11652 (1999).
- [7] M. R. Wilson, P. D. Duncan, M. Dennison, and A. J. Masters, Molecular dynamics simulation studies of platelets with square cross-sectional area: Formation of a stable cubatic phase, *Soft Matter* **8**, 3348 (2012).
- [8] S. D. Peroukidis and A. G. Vanakaras, Phase diagram of hard board-like colloids from computer simulations, *Soft Matter* **9**, 7419 (2013).
- [9] M. Delhomme, C. Labbez, and B. Jonsson, Liquid crystal phases in suspensions of charged plate-like particles, *J. Phys. Chem. Lett.* **3**, 1315 (2012).
- [10] M. Delhomme, B. Jönsson, and C. Labbez, Monte Carlo simulations of a clay inspired model suspension: The role of rim charge, *Soft Matter* **8**, 9691 (2012).
- [11] Y. Martínez-Ratón and E. Velasco, Effect of polydispersity, bimodality, and aspect ratio on the phase behavior of colloidal platelet suspensions, *J. Chem. Phys.* **137**, 134906 (2012).
- [12] R. J. Bushby and O. R. Lozman, Discotic liquid crystals 25 years on, *Curr. Opin. Colloid Interface Sci.* **7**, 343 (2002).
- [13] P. Huber, Soft matter in hard confinement: Phase transition thermodynamics, structure, texture, diffusion and flow in nanoporous media, *J. Phys. Condens. Matter* **27**, 103102 (2015).
- [14] M. M. Piñeiro, A. Galindo, and A. O. Parry, Surface ordering and capillary phenomena of confined hard cut-sphere particles, *Soft Matter* **3**, 768 (2007).
- [15] P. Poier, S. A. Egorov, C. N. Likos, and R. Blaak, Concentration-induced planar-to-homeotropic anchoring transition of stiff ring polymers on hard walls, *Soft Matter* **12**, 7983 (2016).
- [16] F. Barmes and D. J. Cleaver, Computer simulation of a liquid-crystal anchoring transition, *Phys. Rev. E* **69**, 061705 (2004).
- [17] H. Reich and M. Schmidt, Capillary nematization of hard colloidal platelets confined between two parallel hard walls, *J. Phys.: Condens. Matter* **19**, 326103 (2007).
- [18] L. Bellier-Castella, D. Caprion, and J.-P. Ryckaert, Surface ordering of diskotic liquid crystals, *J. Chem. Phys.* **121**, 4874 (2004).
- [19] J. G. Gay and B. J. Berne, Modification of the overlap potential to mimic a linear site-site potential, *J. Chem. Phys.* **74**, 3316 (1981).
- [20] L. Harnau and S. Dietrich, Wetting and capillary nematization of binary hard-platelet and hard-rod fluids, *Phys. Rev. E* **66**, 051702 (2002).
- [21] C. Avendaño, G. Jackson, and H. H. Wensink, Nanorings in planar confinement: The role of repulsive surfaces on the formation of lacuna smectics, *Mol. Phys.* **116**, 2901 (2018).
- [22] M. Schoen, D. J. Diestler, and J. H. Cushman, Stratification-induced order-disorder phase transitions in molecularly thin confined films, *J. Chem. Phys.* **101**, 6865 (1994).
- [23] M. Schoen, D. J. Diestler, and J. H. Cushman, Fluids in micropores. I. Structure of a simple classical fluid in a slit-pore, *J. Chem. Phys.* **87**, 5464 (1987).
- [24] D. J. Diestler, M. Schoen, J. E. Curry, and J. H. Cushman, Thermodynamics of a fluid confined to a slit pore with structured walls, *J. Chem. Phys.* **100**, 9140 (1994).
- [25] M. R. Khadilkar and F. A. Escobedo, Phase behavior of polyhedral nanoparticles in parallel plate confinement, *Soft Matter* **12**, 1506 (2016).
- [26] M. Schoen, The impact of discrete wall structure on stratification-induced structural phase transitions in confined films, *J. Chem. Phys.* **105**, 2910 (1996).
- [27] S. Nasirimoghdam, M. Moradi, and R. Aliabadi, Biaxial planar nematic layered structures of highly confined prolate hard ellipsoids, *Phys. A: Stat. Mech. Appl.* **598**, 127371 (2022).
- [28] H. Salehi, S. Mizani, R. Aliabadi, and S. Varga, Biaxial layering transition of hard rodlike particles in narrow slitlike pores, *Phys. Rev. E* **98**, 032703 (2018).
- [29] S. Mizani, R. Aliabadi, H. Salehi, and S. Varga, Orientational ordering and layering of hard plates in narrow slitlike pores, *Phys. Rev. E* **100**, 032704 (2019).
- [30] F. Behzadi, S. M. Ghazi, and R. Aliabadi, From n -layer planar ordering to the monolayer homeotropic structure of confined hard rods: The effect of shape anisotropy and wall-to-wall separation, *Phys. Rev. E* **103**, 022702 (2021).
- [31] R. van Roij, M. Dijkstra, and R. Evans, Interfaces, wetting, and capillary nematization of a hard-rod fluid: Theory for the Zwanzig model, *J. Chem. Phys.* **113**, 7689 (2000).
- [32] M. Dijkstra, R. van Roij, and R. Evans, Wetting and capillary nematization of a hard-rod fluid: A simulation study, *Phys. Rev. E* **63**, 051703 (2001).
- [33] G. Rickayzen, A model for the study of the structure of hard molecular fluids, *Mol. Phys.* **95**, 393 (1998).
- [34] K. Shundyak and R. van Roij, Isotropic-nematic transition in hard-rod fluids: Relation between continuous and restricted-orientation models, *Phys. Rev. E* **69**, 041703 (2004).

- [35] J. D. Parsons, Nematic ordering in a system of rods, *Phys. Rev. A* **19**, 1225 (1979).
- [36] S. Lee, The Onsager-type theory for nematic ordering of finite-length hard ellipsoids, *J. Chem. Phys.* **89**, 7036 (1988).
- [37] T. Santos-Silva, P. I. C. Teixeira, C. Anquetil-Deck, and D. J. Cleaver, Neural-network approach to modeling liquid crystals in complex confinement, *Phys. Rev. E* **89**, 053316 (2014).
- [38] M. González-Pinto, Y. Martínez-Ratón, S. Varga, P. Gurin, and E. Velasco, Phase behaviour and correlations of parallel hard squares: From highly confined to bulk systems, *J. Phys.: Condens. Matter* **28**, 244002 (2016).
- [39] R. Zwanzig, First-order phase transition in a gas of long thin rods, *J. Chem. Phys.* **39**, 1714 (1963).
- [40] R. Aliabadi, P. Gurin, E. Velasco, and S. Varga, Ordering transitions of weakly anisotropic hard rods in narrow slitlike pores, *Phys. Rev. E* **97**, 012703 (2018).
- [41] J. Herzfeld, A. E. Berger, and J. W. Wingate, A highly convergent algorithm for computing the orientation distribution functions of rodlike particles, *Macromolecules* **17**, 1718 (1984).
- [42] K. W. Wojciechowski and D. Frenkel, Tetratic phase in the planar hard square system? *Comput. Methods Sci. Technol.* **10**, 235 (2004).
- [43] A. Donev, J. Burton, F. H. Stillinger, and S. Torquato, Tetratic order in the phase behavior of a hard-rectangle system, *Phys. Rev. B* **73**, 054109 (2006).
- [44] S. Mizani, P. Gurin, R. Aliabadi, H. Salehi, and S. Varga, Demixing and tetratic ordering in some binary mixtures of hard superellipses, *J. Chem. Phys.* **153**, 034501 (2020).
- [45] J.-C. P. Gabriel and P. Davidson, Mineral liquid crystals from self-assembly of anisotropic nanosystems, in *Colloid Chemistry I* (Springer, Berlin, 2003), pp. 119–172.
- [46] J. P. F. Lagerwall, C. Schütz, M. Salajkova, J. Noh, J. Hyun Park, G. Scalia, and L. Bergström, Cellulose nanocrystal-based materials: From liquid crystal self-assembly and glass formation to multifunctional thin films, *NPG Asia Mater.* **6**, e80 (2014).
- [47] P. Gurin, G. Odriozola, and S. Varga, Enhanced two-dimensional nematic order in slit-like pores, *New J. Phys.* **23**, 063053 (2021).
- [48] K. Praefcke, B. Kohne, B. Gündogan, D. Singer, D. Demus, S. Diele, G. Pelzl, and U. Bakowsky, News on nematic-biaxial liquid crystals, *Mol. Cryst. Liq. Cryst.* **198**, 393 (1991).
- [49] S. Dhara, J. K. Kim, S. M. Jeong, R. Kogo, F. Araoka, K. Ishikawa, and H. Takezoe, Anchoring transitions of transversely polar liquid-crystal molecules on perfluoropolymer surfaces, *Phys. Rev. E* **79**, 060701(R) (2009).
- [50] Y. Martínez-Ratón, Bulk inhomogeneous phases of anisotropic particles: A fundamental measure functional study of the restricted orientations model, *Phys. Rev. E* **69**, 061712 (2004).
- [51] H. Hansen-Goos and K. Mecke, Fundamental Measure Theory for Inhomogeneous Fluids of Nonspherical Hard Particles, *Phys. Rev. Lett.* **102**, 018302 (2009).
- [52] H. Hansen-Goos and K. Mecke, Tensorial density functional theory for non-spherical hard-body fluids, *J. Phys.: Condens. Matter* **22**, 364107 (2010).
- [53] R. Wittmann, M. Marechal, and K. Mecke, Fundamental measure theory for non-spherical hard particles: Predicting liquid crystal properties from the particle shape, *J. Phys.: Condens. Matter* **28**, 244003 (2016).
- [54] H. Reich, M. Dijkstra, R. van Roij, and M. Schmidt, Entropic wetting and the free isotropic–nematic interface of hard colloidal platelets, *J. Phys. Chem. B* **111**, 7825 (2007).
- [55] D. A. Triplet and K. A. Fichtorn, Monte Carlo simulation of two-dimensional hard rectangles: Confinement effects, *Phys. Rev. E* **77**, 011707 (2008).
- [56] G. Bautista-Carbajal, P. Gurin, S. Varga, and G. Odriozola, Phase diagram of hard squares in slit confinement, *Sci. Rep.* **8**, 8886 (2018).
- [57] M. Schoen, D. J. Diestler, and J. H. Cushman, Fluids in micropores. IV. The behavior of molecularly thin confined films in the grand isostress ensemble, *J. Chem. Phys.* **100**, 7707 (1994).
- [58] T. Beica, S. Frunza, R. Moldovan, M. Giurgea, and M. Tintaru, Stability of some structures in a cholesteric liquid crystal layer for tilted anchoring, *Liq. Cryst.* **13**, 127 (1993).
- [59] R. Aliabadi, S. Nasirimoghadam, and H. H. Wensink, Capillary-driven biaxial planar and homeotropic nematization of hard cylinders, *Phys. Rev. E* **105**, 064704 (2022).
- [60] A. Casey and P. Harrowell, Monte Carlo simulations of a layering transition in hard parallelepipeds, *J. Chem. Phys.* **103**, 6143 (1995).
- [61] B. Ruzicka, E. Zaccarelli, L. Zulian, R. Angelini, M. Sztucki, A. Moussaïd, T. Narayanan, and F. Sciortino, Observation of empty liquids and equilibrium gels in a colloidal clay, *Nat. Mater.* **10**, 56 (2011).
- [62] E. Meneses-Juarez, S. Varga, P. Orea, and G. Odriozola, Towards understanding the empty liquid of colloidal platelets: Vapour–liquid phase coexistence of square-well oblate ellipsoids, *Soft Matter* **9**, 5277 (2013).
- [63] J. K. Kim, F. Araoka, S. M. Jeong, S. Dhara, K. Ishikawa, and H. Takezoe, Bistable device using anchoring transition of nematic liquid crystals, *Appl. Phys. Lett.* **95**, 063505 (2009).